WILEY | Hindawi

Retraction

Retracted: Image Recognition about Stability of Soft Surrounding Rock in Tunnel Based on ILBP Algorithm

Security and Communication Networks

This article has been retracted by Hindawi, as publisher, following an investigation undertaken by the publisher [1]. This investigation has uncovered evidence of systematic manipulation of the publication and peer-review process. We cannot, therefore, vouch for the reliability or integrity of this article.

Please note that this notice is intended solely to alert readers that the peer-review process of this article has been compromised.

Wiley and Hindawi regret that the usual quality checks did not identify these issues before publication and have since put additional measures in place to safeguard research integrity.

We wish to credit our Research Integrity and Research Publishing teams and anonymous and named external researchers and research integrity experts for contributing to this investigation.

The corresponding author, as the representative of all authors, has been given the opportunity to register their agreement or disagreement to this retraction. We have kept a record of any response received.

References

[1] Z. Lang, X. Gao, Y. Jia et al., "Image Recognition about Stability of Soft Surrounding Rock in Tunnel Based on ILBP Algorithm," *Security and Communication Networks*, vol. 2022, Article ID 8775881, 9 pages, 2022.

WILEY | Hindawi

Research Article

Image Recognition about Stability of Soft Surrounding Rock in Tunnel Based on ILBP Algorithm

Zhijun Lang,[1] **Xinqiang Gao** ,**[2,3,4]** **Yibin Jia,**[1] **Beiyi Dong,**[2,4] **Zecheng Ma,**[2,4] **Daoyuan Ren,**[2,4] **and Kaza Mojtahe** [5]

[1]*China Construction Seventh Engineering Division Corp. Ltd., Zhengzhou, Henan 450016, China*
[2]*State Key Laboratory of Mechanics Behavior and System Safety of Traffic Engineering Structures, Shijiazhuang Tiedao University, Shijiazhuang, Hebei 050043, China*
[3]*Hebei Province Technical Innovation Center of Safe and Effective Mining of Metal Mines, Shijiazhuang, Hebei 050043, China*
[4]*School of Civil Engineering, Shijiazhuang Tiedao University, Shijiazhuang, Hebei 050043, China*
[5]*Department of Computer Engineering, Kyrgyz-Turkish Manas University, Bishkek, Kyrgyzstan*

Correspondence should be addressed to Xinqiang Gao; gaoxinqiang2020@163.com and Kaza Mojtahe; kaza.mojtahe@ mail.cu.edu.kg

With China's fast expansion of urban traffic and railway engineering, a great number of subway and railway lines have been erected in subterranean tunnels in recent years. When the tunnel is in the process of construction, it will encounter the weak fracture zone, and the surrounding rock of this part of the tunnel is often poor stability and deformation is difficult to control, which will lead to the smooth progress of the project, delay and other problems. Therefore, to facilitate the timely treatment of tunnel soft surrounding rock, the study of image recognition of its stability is particularly important. Based on this, an improved local binary mode algorithm (ILBP) is proposed in this paper. By adjusting the weight of binary polynomial in local binary mode (LBP) operator, the target of ILBP is to extract the characteristics of weak surrounding rock of tunnel at a specific location, hoping to provide reference for the follow-up study of tunnel engineering.

1. Introduction

With the progress of science and technology and the development of society, the construction scale of tunnel engineering is increasing day by day, which greatly facilitates people's travel and life, and its safety is very important. In the process of tunnel construction, it is inevitable to encounter some relatively weak overall strength, prone to large deformation of the construction of rock, which will bring great influence on the stability of the overall tunnel, but also bring serious harm to the transportation. In the operation process of the tunnel, due to the vibration of the vehicle, the disturbance of the surrounding load, and the change of surrounding rock pressure, it is necessary to identify the image of the stability of the weak surrounding rock of the tunnel, which will provide the tunnel maintenance department with

reliable data to carry out maintenance and early warning [1]. Traditional tunnel soft surrounding rock detection has been mostly manual for a long time, with technicians building up scaffolding, artificial inspection with the naked eye, or taking pictures of the tunnel and looking for cracks in the photographs. However, there are also many shortcomings. For the former, the personnel safety problem is a great hidden danger. If the test is carried out on the train, considering that the blank time of the tunnel line is very limited, and the technicians work very hard to complete the test within the limited time, which finally leads to low detection efficiency. The quality of the latter directly affects the detection results, and it is likely to be affected by external factors such as uneven illumination and distortion of line-array camera shooting [2]. Therefore, for these two methods, the accuracy of detection completely depends on the professional level

and quality of technical personnel, and the measurement results of different personnel are not the same. There are strong subjectivity and low efficiency defects. Therefore, manual detection method cannot meet the requirements of tunnel detection; it is imperative to find an objective, accurate, and efficient detection method.

In recent years, with the rapid development of computer technology, the application of machine vision technology in detection has expanded, and the image recognition of the stability of tunnel soft surrounding rock using image detection technology has also received people's attention [3]. This method has many advantages that manual detection does not have. First, this kind of detection is long-distance noncontact detection, does not cause damage to the tunnel surface, and ensures the safety of technicians. Second, through the improved LBP algorithm, the accuracy of detection can be controlled in a large range, and it can be automatically recognized and classified. In addition, this is a completely objective detection method, avoiding the technical personnel's personal mental, fatigue, vision, physical, and other conditions of their own interference. Because of its many advantages and technical support, this method has great development potential in tunnel soft surrounding rock detection [4].

2. Research Status of Weak Surrounding Rock of Tunnel

2.1. Stability Status of Tunnel Surrounding Rock. The complexity of rock mass structure indicates the damage degree of rock mass. When excavating and unloading rock mass, rock mass disturbance and even failure have occurred in different degrees, and the failure law is different from the complete failure law of rock mass. Then, the rule will be largely the constraints of the rock mass structure. Due to the influence of excavation method and support structure, the deformation modes of rock mass are diversified, so it is impossible to discriminate simply by using the experimental data or law of complete rock material [5]. Because there are many influencing factors, there are considerable differences in the structural characteristics and strength of rock mass. It is these differences that make the instability of weak surrounding rock of deep highway tunnel has the influence of diversified factors. Rock mass changes from brittleness to ductility, and soil rupture and collapse of loose rocks in surrounding rock will lead to serious instability of surrounding rock. When surrounding rock is unloaded, rock mass looseness and expansion will result in instability of surrounding rock due to fragmentation and fracture of layered soil mass. The specific classification is shown in Table 1.

2.2. The Geological Characteristics of Weak Surrounding Rock. The surrounding rock mass is defined as the rock mass whose stress condition changes because of tunnel excavation. Hard surrounding rock and soft surrounding rock may be distinguished based on the strength of the rock mass. It may be classified as grade I–VI surrounding rock

depending on the grade of the surrounding rock. Its stable deformation can be divided into the following three stages, as shown in Figure 1.

Weak surrounding rock usually has the following characteristics.

(1) Low Rock Strength

According to China's "Engineering Rock Mass Classification Standard," "Railway Tunnel Design Code," and other standards, generally, the uniaxial saturation compressive strength of less than 30 MPa rock is called soft rock or soft rock. Soft rocks mainly include nondiagenetic rocks, weathered rocks, and rocks containing soft minerals. Typical rocks include mudstone, sandstone, phyllite, carbonaceous SLATE, and sericite schist.

(2) Rock Fragmentation

Hard rock seriously affected by geological structure can also be called soft surrounding rock. If the hard rock is affected by strong tectonic movement, which leads to the development of joints, fissures, faults, and other structural planes, the strength of surrounding rock will be reduced, and the self-stability will become poor.

(3) Poor Occurrence Environment of Surrounding Rock

Once the surrounding rock of tunnel exists in poor geological environment such as rich water and high ground stress, it is easy to cause geological disasters such as water gushing and collapse. The surrounding rock occurring in these unfavorable geological environments can also be called weak surrounding rock.

2.3. Deformation Characteristics of Soft Surrounding Rock in Tunnel

(1) There is a large range of surrounding rock deformation in front of the palm of the weak surrounding rock. Generally, the deformation range of surrounding rock at the front hard surrounding rock palm is very small. The deformation of surrounding rock within the range of one time of aperture is very small and can be ignored [6]. In front of the soft surrounding rock, there is a large range of deformation. The collapse deformation phenomenon will gradually expand the deformation range of the surrounding rock in front, even to three or four times the aperture range.

(2) A considerable amount of the deformation occurs in front of the soft surrounding rock. The deformation of the rock in front of the palm face generally accounts for 20% of the overall deformation in typical hard rock. The deformation in front of the soft surrounding rock, on the other hand, will account for 30 percent of the overall deformation, if not more. The soft surrounding rock will be a crucial element in deformation or collapse of the palm face vault if it is not managed.

TABLE 1: Grade of surrounding rock.

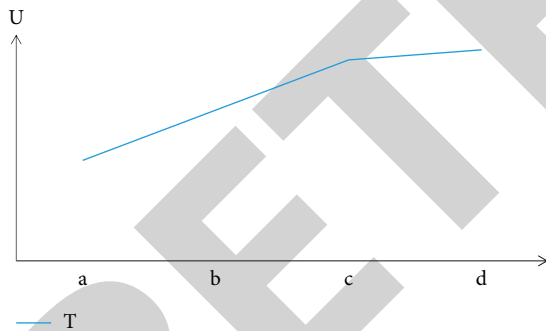| The level of surrounding rock	Main qualitative characteristics of surrounding rock or soil	Basic quality index of surrounding rock (BQ) or modified basic quality index of surrounding rock [BQ]
I	Hard rock, rock integrity, giant monolithic or thick bedded structure	>550
II	Hard rock, rock integrity, massive or thick bedded structure More hard rock, complete rock mass, massive overall structure	550–451
III	Hard rock, rock mass is broken, huge block (stone) broken (stone) mosaic structure, harder rock or more soft and hard rock, rock mass is more complete, massive or thick layer structure	450–351
IV	Hard rock, fractured rock mass, cataclysmic structure More hard rock, rock mass more broken ~ broken, mosaic fracture structure Soft rock or interbedded soft and hard rock, and mainly soft rock, the rock mass is more complete ~ more broken, medium thin bedded structure Soil: ① compacted or diagenetic cohesive soil and sandy soil; ② loess (Q1, Q2); ③ general calcium, iron cemented gravel soil, pebble soil, large stone soil	350–251
V	Soft rock, rock fragmentation; soft rock, rock mass is broken ~ broken; extremely broken all kinds of rock mass. Broken, cracked, loose structure Generally, quaternary semidry clay to hard plastic clay and slightly wet to wet gravel soil, pebble soil, gravel, brecciated soil and loess (Q3, Q4). Noncohesive soil has loose structure, clay soil and loess have soft structure	≤250
VI	Soft plastic clay and wet, saturated fine sand layer, soft soil, etc.	

FIGURE 1: Three stages of stable deformation of surrounding rock. U: deformation displacement of surrounding rock (mm); T deformation time of surrounding rock (s); ab: stage of rapid deformation; bc: slow deformation stage; cd: basically stable stage.

(3) There is a very obvious extrusion deformation in the face of the soft surrounding rock, and there is a certain relationship between the geological tendency and the angle between the highway tunnels. When the included angle is acute, the range of extrusion deformation is 1~1.3 times of hole diameter. If the included angle is obtuse, the extrusion deformation range will be approximately 1.2~1.6 times the hole diameter size.

(4) The rear deformation range of weak surrounding rock is large, so if there is not scientific and effective support and reinforcement of weak surrounding rock, it will lead to continuous expansion of surrounding rock deformation, until the surrounding rock loses stability, collapse phenomenon.

3. ILBP Algorithm Overview

LBP operator was first proposed by Ojala et al., machine vision research group of University of Oulu, Finland, based on texture spectrum method. Because of its simple calculation principle, low complexity, and easy to integrate with other features such as strength, LBP operator has been expanded in an endless stream since its emergence. The method is also widely used in face recognition, image segmentation, target tracking and medical image analysis, and other fields [7].

The LBP method is a basic yet efficient texture feature extraction and representation approach with minimal computing cost and gray level invariance. As a result, picture matching, recognition, and classification are all common applications. Rotation invariance was not present in the original LBP operator. With its improvement, the application field of LBP algorithm was further broadened and began to be applied to texture extraction of high-resolution remote sensing images, biomedical image analysis, and motion detection. The extended LBP algorithm achieves good results in real-time vehicle detection, image segmentation, and face recognition due to its advantages in precision and computation. Therefore, this paper adopts the improved LBP
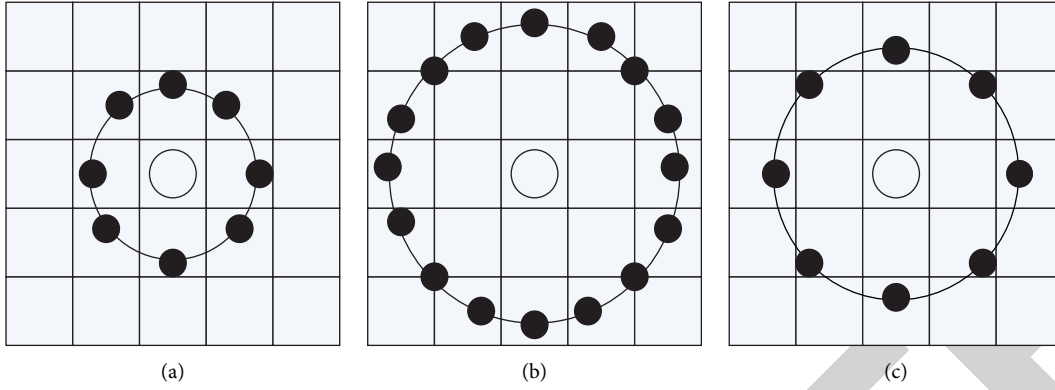
Figure 2: Examples of LBP operators. (a) LBP_8^1. (b) LBP_{16}^2. (c) LBP_8^2.
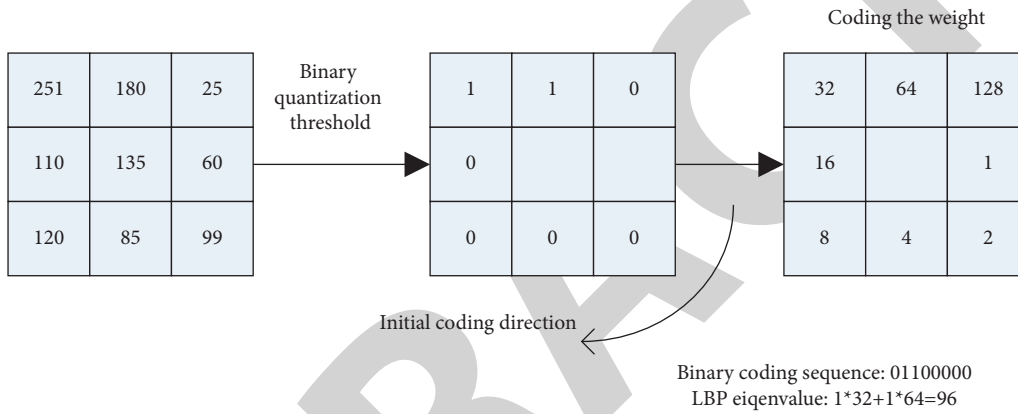

Figure 3: Eigenvalue calculation of the original LBP operator.

algorithm to identify the stability of tunnel soft surrounding rock.

3.1. LBP Descriptor. LBP operators are mainly classified as follows, as shown in Figure 2.

LBP operator was originally defined on a 3×3 rectangular neighborhood system centered on any pixel in a gray image. By taking the gray value of the central pixel in the local neighborhood as the threshold value, the relationship between the gray level of each pixel in the neighborhood and the threshold value was binary quantified one by one. The binary quantized sequence is numerically converted to generate the eigenvalues used to describe the local texture of the image, as shown in Figure 3 [8]. The neighborhood system a 3×3 rectangle indicates the binary quantization relationship between the gray level difference between the neighborhood pixel and the central pixel. If the gray difference of the pixels in the rectangular neighborhood and the binary quantization threshold are not negative, the pixels in the corresponding position are marked as 1, otherwise set as 0, and different weights are given to different neighborhood points according to the given coding direction [9]. The unsigned decimal value of the quantized binary coding sequence is subsequently employed as the LBP characteristic mode value of the associated pixel point.

3.2. Advantages and Disadvantages of ILBP Method

3.2.1. Advantages of ILBP Algorithm

(1) The theory is simple and clear and easy to understand, the calculation process is convenient and fast, and it is very easy to realize from the perspective of coding [10]. To sum up, ILBP-based methods require only simple template operation and histogram vector generation. Compared with other methods, ILBP-based methods require less computation [11]. From the perspective of classification, this advantage brings about a significant reduction in training cost and an improvement in classification speed.

(2) Strong ability of feature classification, ILBP can not only describe some small features in the image, including bright spots, dark spots, stable regions, and edges in all directions, but also reflect the distribution of these features [12]. In addition, ILBP has arbitrary monotone transformation invariance and image rotation invariance. At the same time, compared with the ILBP code corresponding to a pixel, the correlation between the pixel and the surrounding pixels is added, which can better characterize the image features and reduce the influence of illumination changes and angle changes on feature

FIGURE 4: Improved schematic diagram of weight operator. (a) LBP weight. (b) ILBP weight.

extraction [13]. Undoubtedly, these advantages make ILBP features have strong classification ability.

3.2.2. Shortcomings of ILBP Algorithm.

Although ILBP method has the advantages mentioned above, it also has some disadvantages from the classification point of view.

(1) For all issues, use a single transformation mapping. We can observe from the ILBP study that ILBP characteristics are often extracted in the same manner [14]. A single fixed feature is represented by a feature. Clearly, such feature representation is incompatible with the search for categorised hyperplane.

(2) Regarding sensitivity to noise, the ILBP codes of neighboring regions are not independent of each other, but related to their neighboring points, so ILBP is sensitive to noise [15].

(3) In the process of texture analysis, the window size of ILBP method is fixed and irrelevant to image content, which leads to errors in the extraction of texture primitive features by ILBP and makes it difficult to adapt to the requirements of different roughness and scale textures.

3.3. ILBP Algorithm.

The traditional LBP algorithm has rotation invariance. To make the traditional LBP algorithm have the ability to highlight the direction feature, this paper improves it and proposes ILBP algorithm [16]. LBP operator within the neighborhood center pixel (radius 3 tiles) to be encoded in binary order and weak rock tunnel in the image reflects the main texture features, analysis of the texture to a current, which can identify the stability of the weak rock tunnel in order to highlight its texture feature, the direction of pixels to adjust the weights of operator. The result is shown in Figure 4.

The ILBP computing framework is shown in Figure 5. ILBP algorithm is calculated as follows [17]:

$$
\begin{aligned}
\text{ILBP} = (x_c, y_c) = {} & s(g_0, g_c) \cdot 2^7 + s(g_1, g_c) \cdot 2^0 \\
& + s(g_2, g_c) \cdot 2^5 + s(g_3, g_c) \cdot 2^1 + s(g_4, g_c) \cdot 2^4 \quad (1) \\
& + s(g_5, g_c) \cdot 2^3 + s(g_6, g_c) \cdot 2^6 + s(g_7, g_c) \cdot 2^2.
\end{aligned}
$$

4. Experiment and Result Analysis

4.1. Image Acquisition.

A rapid image acquisition system of tunnel surface is designed for the image acquisition of tunnel soft surrounding rock using a multilens high-speed and high-resolution camera, which synchronises image acquisition at high speed, realises tunnel surface image shooting, and performs mobile image data storage [18]. Considering the tunnel imaging environment and cost performance requirements, high-speed industrial linear array camera, optical lens, image acquisition card, light source, and other components are selected to meet the requirements of high-speed and high-precision system. According to the system design, a multicamera and multilight source high-speed tunnel crack movement detection subsystem is built to collect and store the simulated tunnel crack images.

The functions of each device are described as follows.

(1) High-speed industrial line-array camera: conduct row by row continuous scanning of the soft surrounding rock of the tunnel simulated in the laboratory to obtain high-resolution tunnel surface images, making preparation for further image processing and texture feature extraction.

(2) Optical lens: select the focal length and adjust the aperture and other parameters according to the actual environmental distance to meet the requirements of the camera, achieve accurate focusing, and ensure clear camera imaging [19].

(3) Image acquisition card: the image signal of tunnel soft surrounding rock obtained by high-speed industrial camera is collected, converted, and transmitted to the computer in real time, and the digital
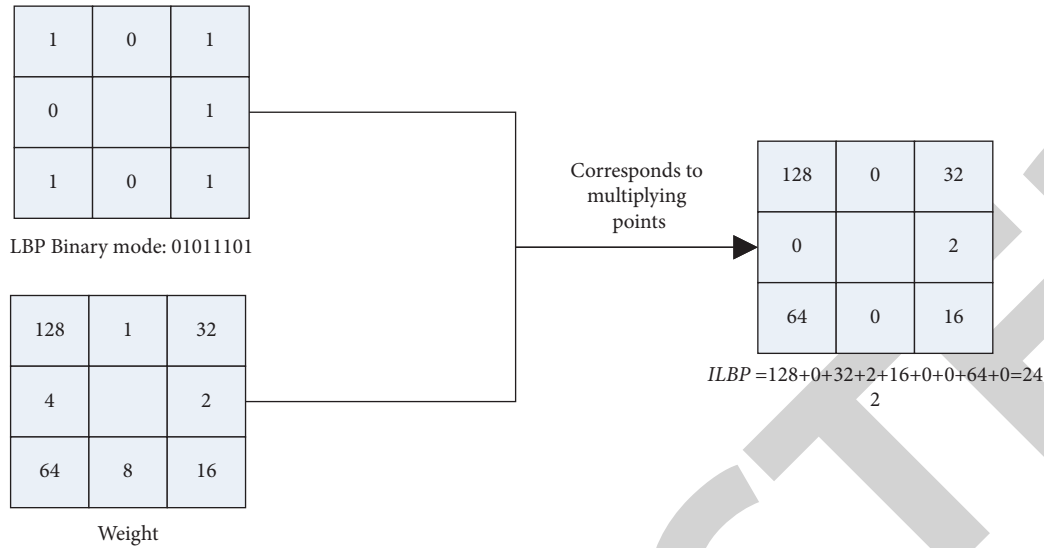
Figure 5: Schematic diagram of ILBP value calculation.

image signal is stored in the hard disk of the computer.

(4) Light source: it provides good lighting support for high-speed industrial cameras and ensures sufficient light during image acquisition. For different environments, it is necessary to select specific light sources to achieve high quality image acquisition.

(5) Mechanical detection vehicle: a collection device with compact structure and precision adjustment is designed to ensure the accurate coordination of multiroute array camera and linear light source and to collect high-resolution images with clear texture and uniform gray scale, laying a foundation for the subsequent high-precision stability detection of tunnel soft surrounding rock.

(6) Computer: supporting software displays the tunnel images collected by the camera in real time to assist in the accurate focusing of the camera; the acquisition software sets the frame number to obtain the corresponding tunnel images and stores the massive images of soft surrounding rock transmitted by the image acquisition card [20]. The algorithm is studied and tested, and the crack images collected are preprocessed, filtered, and segmented, so as to realize the automatic identification of the stability of soft surrounding rock.

(7) Power supply system: provide power supply support for the whole system. Among them, the image acquisition card needs 5 V DC, camera, light source, computer needs 220 V DC.

4.2. The Experimental Process

4.2.1. Determination of Training Model and Test Sample Characteristics. The training model is generally obtained by integrating multiple training samples, but the number and selection of training samples will affect the subsequent image

recognition effect. To obtain the training model, the training samples need to be divided into good samples, boundary samples, and poor samples. The model trained with good samples can narrow the region of this class, the interval between different types of regions will be larger, and the same kind will be closer. If too many good samples are used, the misunderstanding of boundary samples and poor samples will greatly affect the recognition process. However, the difference samples tend to cause classification errors in the training model, because their existence makes two or more regions of different classes overlap, which leads to the training pattern class region becoming larger. At this time, boundary samples are used for model training, so that the training model can make the secant lines of different class regions not coincide as much as possible while the class region is large enough, so as to lay a foundation for the best classification effect. However, using too many feature dimensions leads to time complexity and unsatisfactory recognition effect. A good training model should have the characteristics of using less classification conditions and achieving the best classification effect. The determination process of training model is as follows:

Step 1. First, the HISTOGRAM distribution of ILBP under multiple scale blocks was obtained. Then, the histogram of all training samples under the same scale block was superimposed and the mean value was calculated.

Step 2. It can be seen from Figure 4 that the number of ILBP $(8, 1) = 0$ or 255 modes in the texture image is large and has no obvious effect on classification. The corresponding number of these two ILBP operators is set to 0 and marked as invalid features.

Step 3. Select the most representative, that is the first N ILBP operators with a large number, from the mean of training samples under each scale block, and their corresponding numbers constitute the training model. Table 2 shows the first six feature components of the

training model when it is divided into 2×2 blocks, that is, the corresponding statistical quantities of ILBP values.

The determination process of test sample features is as follows.

Step 1. Obtain ILBP histogram of test sample in each scale block.

Step 2. When matching measurement with the training model, the number of test samples under the same ILBP with the training model at the same scale is taken as feature vector. Table 3 shows the statistical quantity of test samples with the same ILBP value under training model 3.

4.2.2. Texture Image Classification. Assess if the difference between the test sample's characteristics and the training model's characteristics is within a tolerable range after obtaining the training model's and test sample's characteristics. If so, add 1 to the matching similarity; otherwise, the feature does not contribute to the matching. At the same time, considering the different size of the difference between the characteristics of the test sample and the training model, the reasonable range should be determined according to the size of the block. The smaller the block, the more ILBP, and the difference can be slightly amplified. The larger the blocks are, the smaller the number of ILBP is, and the difference value needs to be slightly smaller. The reasonable range of the difference value is defined as $1000/n^2$. However, since the contribution of different scale blocks to feature extraction is inconsistent, the measurement values at different scales need to be weighted to get the final matching result. The ILBP statistical histogram is shown in Figure 6.

4.3. The Experimental Process. To evaluate the effectiveness of the algorithm proposed in this paper, images of 25 texture features in the database are used. Each texture image has 40 samples, and each sample is composed of $640 * 480$ images. The first 20 samples in each category were selected as training samples, and all images were selected as test samples. The experimental process is shown in Figure 7. First, the image is preprocessed, and then, feature extraction is carried out on the input image to determine the feature vector of the test sample and the trained ILBP model, and the training model is used to match the test sample, and the final recognition result is determined according to the similarity degree, and the recognition accuracy is counted.

4.4. Measure and Match. ILBP texture map is also called ILBP map after an image is processed by ILBP operator. However, ILBP map cannot be directly used as the feature vector of the image. In general, the statistical histogram of ILBP Atlas is used to represent the features of the image, and then, the similarity measurement function is used to calculate the ILBP statistical histogram of the two samples to compare their similarity. In the ILBP statistical histogram, the horizontal coordinate represents the number of

Table 2: 6 characteristics of the training model.

Characteristics of the component	1	2	3	4	5	6
ILBP value	60	195	120	30	135	124
Statistics of the number	2874	2108	1916	1523	1496	1373

Table 3: Test sample features extracted from the training model.

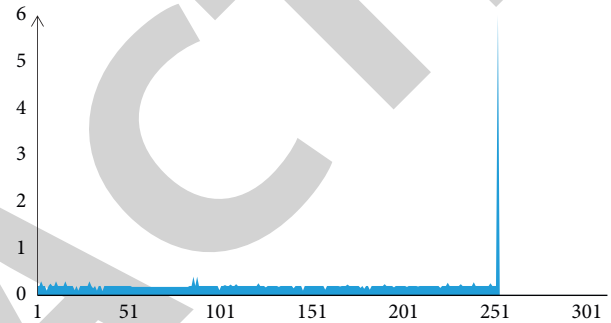| Characteristics of the component	1	2	3	4	5	6
ILBP value	60	195	120	30	135	124
Statistics of the number	1957	2204	425	2505	423	676

Figure 6: ILBP statistical histogram. The vertical axis is the number of mode values/$\times 10^6$.

categories of ILBP mode values (in a 3×3 window, the types of ILBP mode values are 256, that is, the total Bin number is 256), and the vertical coordinate represents the number of pixels of this ILBP mode value. Among all kinds of LBP statistical histogram similarity measures, the similarity measure function commonly used is chi statistical method, that is, to calculate the deviation between the actual value and the theoretical value. The actual value can be regarded as a $\times 256$ matrix successively composed of ordinates in the ILBP statistical histogram of the test image, and the theoretical value is a 1×256 matrix successively composed of ordinates in the ILBP statistical histogram of the image in the reference database. The formula of chi statistics can be expressed as

$$x^2(S, M) = \sum_{b=1}^{B} \frac{(S_b - M_b)^2}{(S_b + M_b)}, \tag{2}$$

where S and M are histogram matrices of the tested samples and training samples respectively, S_b and M_b are the number of the BTH Bin of ILBP histogram of the tested samples and classified samples respectively, and B represents the total Bin number of ILBP histogram. The chi statistical method is used to measure the similarity between histograms. The smaller the chi distance between two samples, the more similar the two samples are. The chi statistics were used to perform feature matching with the images in the reference database, and the results were sorted by size of similarity from high to low to find the most similar image of tunnel soft
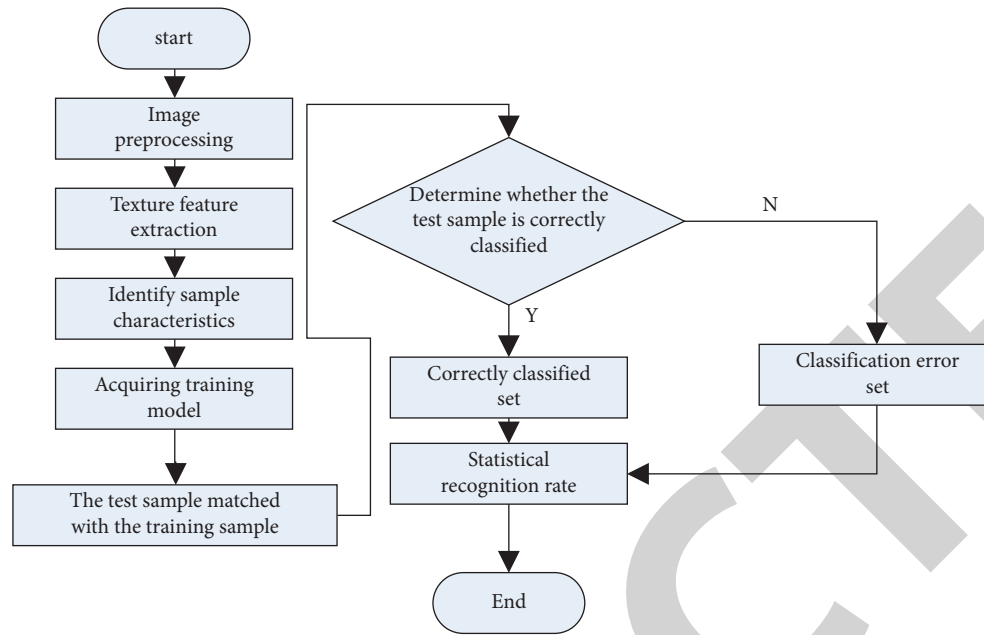
Figure 7: Texture image recogniti4on process.

Table 4: Comparison of LBP and ILBP algorithm results.

Algorithm	POD	FAR	CSI
LBP	0.857	0.182	0.72
ILBP	0.884	0.150	0.76

surrounding rock stability; that is, the image was assigned to the category of the most similar image, and the classification results were obtained.

4.5. Analysis of Experimental Results. A comparative experiment was conducted on the above test datasets, and the experimental results are as follows:

(1) LBP algorithm: the correct times of prediction is 144 times, the missed times is 24 times, and the false times is 32 times.

(2) ILBP algorithm: the correct prediction times were 153 times, the missed prediction times were 20 times, and the false prediction times were 27 times. POD, FAR, and CSI values of LBP and ILBP algorithms were calculated according to the experimental results, and the calculation results are shown in Table 4.

Table 4 shows that all evaluation indexes of ILBP algorithm are superior. The original LBP algorithm has high accuracy and reliability.

5. Conclusion

To better realize the study of the stability of tunnel soft surrounding rock, this paper summarizes the existing feature extraction algorithm and classification algorithm and analyzes their advantages and disadvantages and research

status. For its exceptional performance in texture features, the LBP operator has been extensively employed in various aspects of machine vision. This study provides a more beneficial ILBP method based on the fundamental LBP operator to determine the stability of weak surrounding rock. In this paper, the actual application effect of the existing LBP algorithm and ILBP algorithm is compared. The results show that the algorithm in this paper is better than the LBP algorithm in each evaluation index, and its accuracy and reliability reach the standard of artificial prediction. It provides some reference for the follow-up research.

The ILBP algorithm studied in this paper solves the problem of inconvenient and timely detection of tunnel broken zone in tunnel engineering in image recognition of stability of weak surrounding rock to a certain extent. However, it still has some shortcomings, and its image recognition is not intelligent enough, which needs further research.

Data Availability

The data used to support the findings of this study are included within the article.

Conflicts of Interest

The authors declare that they have no conflicts of interest.

Acknowledgments

References

[1] Z. Zhang, X. Shi, B. Wang, and H. Li, "Stability of NATM tunnel faces in soft surrounding rocks," *Computers and Geotechnics*, vol. 96, pp. 90–102, 2018.

[2] G. Cui, J. Qi, and D. Wang, "Experimental study on load bearing characteristics of steel fiber reinforced concrete lining in the soft surrounding rock tunnel," *Advances in Civil Engineering*, vol. 2020, Article ID 4976238, 12 pages, 2020.

[3] X. Sun, B. Zhang, L. Gan, Z. Tao, and C. Zhao, "Application of constant resistance and large deformation anchor cable in soft rock highway tunnel," *Advances in Civil Engineering*, vol. 2019, Article ID 4347302, 19 pages, 2019.

[4] Y. Han, X. Liu, D. Li et al., "Model test on the bearing behaviors of the tunnel-type anchorage in soft rock with underlying weak interlayers," *Bulletin of Engineering Geology and the Environment*, vol. 79, no. 2, pp. 1023–1040, 2020.

[5] X. Sun, F. Chen, C. Miao et al., "Physical modeling of deformation failure mechanism of surrounding rocks for the deep-buried tunnel in soft rock strata during the excavation," *Tunnelling and Underground Space Technology*, vol. 74, pp. 247–261, 2018.

[6] Z. Fang, Z. Zhu, and P. Wu, "Excavation and support method of tunnel with high ground stress and weak surrounding rock based on GIS," *Arabian Journal of Geosciences*, vol. 14, no. 7, pp. 1–13, 2021.

[7] F. N. Wang, Z. B. Guo, X. B. Qiao et al., "Large deformation mechanism of thin-layered carbonaceous slate and energy coupling support technology of NPR anchor cable in Minxian Tunnel: a case study," *Tunnelling and Underground Space Technology*, vol. 117, Article ID 104151, 2021.

[8] N. Mohan and N. Varshney, "Facial expression recognition using improved local binary pattern and min-max similarity with nearest neighbor algorithm," *Smart Innovations in Communication and Computational Sciences*, vol. 1168, pp. 309–319, 2021.

[9] S. Goyal, A. Rani, and V. Singh, "An improved local binary pattern based edge detection algorithm for noisy images," *Journal of Intelligent and Fuzzy Systems*, vol. 36, no. 3, pp. 2043–2054, 2019.

[10] S. Srivastava, A. Kumar, and S. Prakash, "Biometric facial detection and recognition based on ILPB and SVM," *Artificial Intelligence and Data Mining Approaches in Security Frameworks*, vol. 8, pp. 129–154, 2021.

[11] G. Kumar, S. Bakshi, P. K. Sa, and B. Majhi, "Non-overlapped blockwise interpolated local binary pattern as periocular feature," *Multimedia Tools and Applications*, vol. 80, no. 11, pp. 16565–16597, 2021.

[12] H. Zhao, Z. Liu, X. Yao, and Q. Yang, "A machine learning-based sentiment analysis of online product reviews with a novel term weighting and feature selection approach," *Information Processing & Management*, vol. 58, no. 5, Article ID 102656, 2021.

[13] S. Inunganbi, P. Choudhary, and K. M. Singh, "Local texture descriptors and projection histogram based handwritten Meitei Mayek character recognition," *Multimedia Tools and Applications*, vol. 79, no. 3-4, pp. 2813–2836, 2020.

[14] W. Zhang, F. Y. Shih, S. Hu, and M. Jian, "A visual secret sharing scheme based on improved local binary pattern," *International Journal of Pattern Recognition and Artificial Intelligence*, vol. 32, no. 6, Article ID 1850017, 2018.

[15] M. H. Shakoor and R. Boostani, "Radial mean local binary pattern for noisy texture classification," *Multimedia Tools and Applications*, vol. 77, no. 16, pp. 21481–21508, 2018.

[16] A. Lati, M. Belhocine, M. Chaa, and N. Achour, "Efficient binary descriptor-based implementation of fuzzy image registration algorithms on LabVIEW," *Journal of Electronic Imaging*, vol. 30, no. 5, Article ID 053023, 2021.

[17] S. G. Tong, Y. Y. Huang, and Z. M. Tong, "A robust face recognition method combining LBP with multi-mirror symmetry for images with various face interferences," *International Journal of Automation and Computing*, vol. 16, no. 5, pp. 671–682, 2019.

[18] R. Thirumalaisamy and S. K. Mohideen, "A study and analysis of improved binary pattern technique in dynamic images," *Turkish Journal of Computer and Mathematics Education (TURCOMAT)*, vol. 12, no. 6, pp. 2602–2608, 2021.

[19] M. U. Nagaral and T. H. Reddy, "Hybrid approach for facial expression recognition using HJDLBP and LBP histogram in video sequences," *International Journal of Image, Graphics and Signal Processing*, vol. 12, no. 2, p. 1, 2018.

[20] F. Bianconi, R. Bello-Cerezo, and P. Napoletano, "Improved opponent color local binary patterns: an effective local image descriptor for color texture classification," *Journal of Electronic Imaging*, vol. 27, no. 1, p. 1, 2017.